

Article

Effects of Pounding and Abutment Behavior on Seismic Response of Multi-Span Bridge Considering Abutment-Soil-Foundation-Structure Interactions

Yulin Deng ^{1,*}, Shuxun Ge ¹ and Fan Lei ²

¹ Department of Road and Bridge Engineering, School of Transportation and Logistics Engineering, Wuhan University of Technology, Wuhan 430063, China

² School of Naval Architecture, Ocean and Energy Power Engineering, Wuhan University of Technology, Wuhan 430063, China

* Correspondence: dengyulin@whut.edu.cn

Abstract: This study aims to analyze the longitudinal seismic performance of a typical multi-span continuous girder bridge with seat-type abutments under earthquake excitation, especially accounting for different abutment behaviors. Three-dimensional finite element models of typical multi-span bridges are built considering the nonlinearity of the bridge columns, bearings, abutment-backfill interactions, pile-soil interactions, and the pounding at expansion joints. One of the models adopts a simplified bilinear model to express the force-displacement relationship of the abutment backwall. The other adopts a more practical multi-linear model, and the abutment backwall is used as a sacrificial component to control the damage to the abutment's foundation by changing the strength of the abutment backwall. Comparisons of the results of the analysis of two bridge models with and without a sacrificial backwall indicate that it is more favorable for bridges with a sacrificial backwall to protect the foundation, but it is likely to arouse a larger displacement response of the main beam and even cause the unseating of girders. The recommendation for a sacrificial abutment in seismic design is that the right yield strength of the backwall should be selected to reach the balance point of force and displacement, and a collapse-proof system could be employed to prevent the beam from unseating.

Keywords: bridge seismic response; non-linear analysis; abutment-backfill interactions; pile-soil interactions; pounding effect



Citation: Deng, Y.; Ge, S.; Lei, F. Effects of Pounding and Abutment Behavior on Seismic Response of Multi-Span Bridge Considering Abutment-Soil-Foundation-Structure Interactions. *Buildings* **2023**, *13*, 260. <https://doi.org/10.3390/buildings13010260>

Academic Editor: Harry Far

Received: 8 December 2022

Revised: 29 December 2022

Accepted: 6 January 2023

Published: 16 January 2023



Copyright: © 2023 by the authors. Licensee MDPI, Basel, Switzerland. This article is an open access article distributed under the terms and conditions of the Creative Commons Attribution (CC BY) license (<https://creativecommons.org/licenses/by/4.0/>).

1. Introduction

Abutments, as a component connecting the ends of bridge spans and embankments, play the role of supporting the superstructure and retaining the soil or rock under normal operations. When a bridge is subjected to seismic loads, however, the main beam moves toward the abutment and collides with it. Earthquake reconnaissance reports demonstrate that abutment damage caused by pounding between the superstructure and abutment is a kind of typical phenomenon, e.g., the 1999 Chi-Chi earthquake, the 2011 Christchurch earthquake, and the 2008 Wenchuan earthquake [1–3], mainly including abutment slope sliding, the loss of foundation bearing capacity, the strength failure of the abutment backwall, and the collapse of backfill. These disasters fully reveal the vulnerability of bridge abutments to seismic-induced pounding.

It is generally recognized that the huge impact between the beam and abutment changes the passive resistance of backfill, resulting in the permanent displacement of soil [4]. Then, the huge pounding force is partially transmitted to the pile foundation through the abutment breast wall, which may give rise to plastic damage to the pile foundation and its surrounding soils. Therefore, the seismic performance of the entire

bridge system becomes highly nonlinear and is greatly dominated by the soil–structure interactions, embankment flexibility, and abutment behavior.

Great attention was paid to the effect of the soil–abutment–foundation–structure interactions on the seismic performance of bridges in recent years. Earlier literature devoted to the analysis of the nonlinear dynamic response of bridges could be broadly divided into two categories depending on the research emphasis of abutment-soil-foundation-superstructure interactions: (i) abutment-backfill interactions. The nonlinear behavior of the abutment–backfill interactions has been shown through experimental studies [5–7] and theoretical studies [8–10]. Shamsabadi et al. built a 3D nonlinear finite element model considering the nonlinear behavior of the abutment and backfill to explore the seismic response of a skewed bridge under bilateral ground motions [11]. Luo et al. introduced a detailed nonlinear finite element model to study abutment–foundation–structure interactions for quasi-isolated bridges [12]. Thomaidis et al. investigated the rocking isolation of bridges considering the abutment–backfill interactions and evaluated the seismic performance of rocking bridges with isolated piers of the same cross section and height [13]; (ii) pile-soil interactions. Two types of analysis models, the finite element model and the discrete spring model, are commonly used to study the responses of loaded piles. The finite element approach treats the soil and piles as a continuum. For example, Liu et al. developed an elastic-plastic solid model to consider the pile-soil-cap interactions of a composite foundation [14]. Basack et al. proposed a novel numerical model to explore the response of a single pile under a cyclic torsional load [15]. Li et al. established a three-dimensional solid model of a pile to study the nonlinear pile-soil interaction responses and derived a formulation of a three-dimensional pile element [16]. On the other hand, the discrete spring model employs spline elements and spring elements to simulate the pile foundations and the surrounding soils, respectively. Phanikanth et al. applied the p - y approach to investigate the seismic response of pile foundations, considering the degradation of p - y backbone curves caused by soil liquefaction [17]. Wang et al. investigated the seismic failure mechanism of elevated pile-cap foundations through quasi-static cyclic lateral loading tests and numerical analysis [18]. Su et al. used the p - y approach to analyze the non-dimensional response of free-head pile foundations under the combined action of lateral forces and bending moments [19].

Previous studies reveal that the seismic performance of bridges is closely linked with the abutment-backfill interactions and pile-soil interactions. These studies only considered part of the nonlinearity of boundary conditions for bridge structures. Moreover, the nonlinearity of bridge components, such as piers, bearings, and the contact nonlinearity of the pounding effect, could also significantly affect the accuracy of the numerical results [20]. The OpenSees platform has a rich and expanding material library and element library to simulate the seismic response of structures. The assembly of the bridge girder and abutment backwall can be modeled in OpenSees with compression-only elements [21]. The previous studies used a simplified force-displacement relationship in the element used to simulate the abutment backwall, which could not reflect the real seismic response of an abutment backwall under earthquake action. This paper aims to develop a bridge model comprehensively considering these nonlinear factors to analyze the longitudinal seismic response of a multi-span bridge with different abutment behavior: one is that the abutment backwall is a linear elastic capacity-protected component with sufficient yield strength; another is that the backwall is a sacrificial component considering its damage and failure mechanisms. Three-dimensional finite element models of the whole bridge are built, including the pounding that occurred at expansion joints between adjacent structures and the nonlinearity of the column and bearing pads, especially the soil-pile interactions and abutment-backfill interactions. A nonlinear time history analysis is conducted to investigate the seismic responses of the multi-span bridge.

2. Bridge Configurations and Modeling

2.1. Benchmark Bridge

The selected bridge is a $(3 \times 30 + 4 \times 30 + 3 \times 30)$ m RC (reinforced concrete) continuous T-beam bridge supported on double-column piers and seat-type abutments. The superstructure, constructed with Chinese Grade C50 concrete with a Young's modulus of 34.5 GPa, is a five-piece reinforced concrete T girder with a height of 2.0 m. Sliding rubber bearings are used at piers P₃ and P₇ (ten bearings) and at abutments (5 bearings). Plate rubber bearings are used at piers P₁, P₂, P₄, P₅, P₆, P₈, and P₉ (five bearings on each pier). The abutment is filled with soft clay, and the abutment backwall is 2.3 m in height and 10.75 m in width. The piers are made up of two circular, reinforced columns with a diameter of 1.5 m, which vary from 3 m to 6 m in height. The pier bottom is provided with a 1.2 m × 1.5 m tie beam, while the pier top has a 1.8 m × 1.5 m cap beam integrated with the deck. The abutments and piers are supported on 3 and 2 cast-in-place bored piles, respectively. Chinese Grade C30 concrete (with a Young's modulus of 30.0 GPa) is used for the cap, tie beam and abutment backwall, and Chinese Grade C30 underwater concrete is used for the bridge's pile foundation. The geometry of the pier columns and abutments is shown in Figure 1.

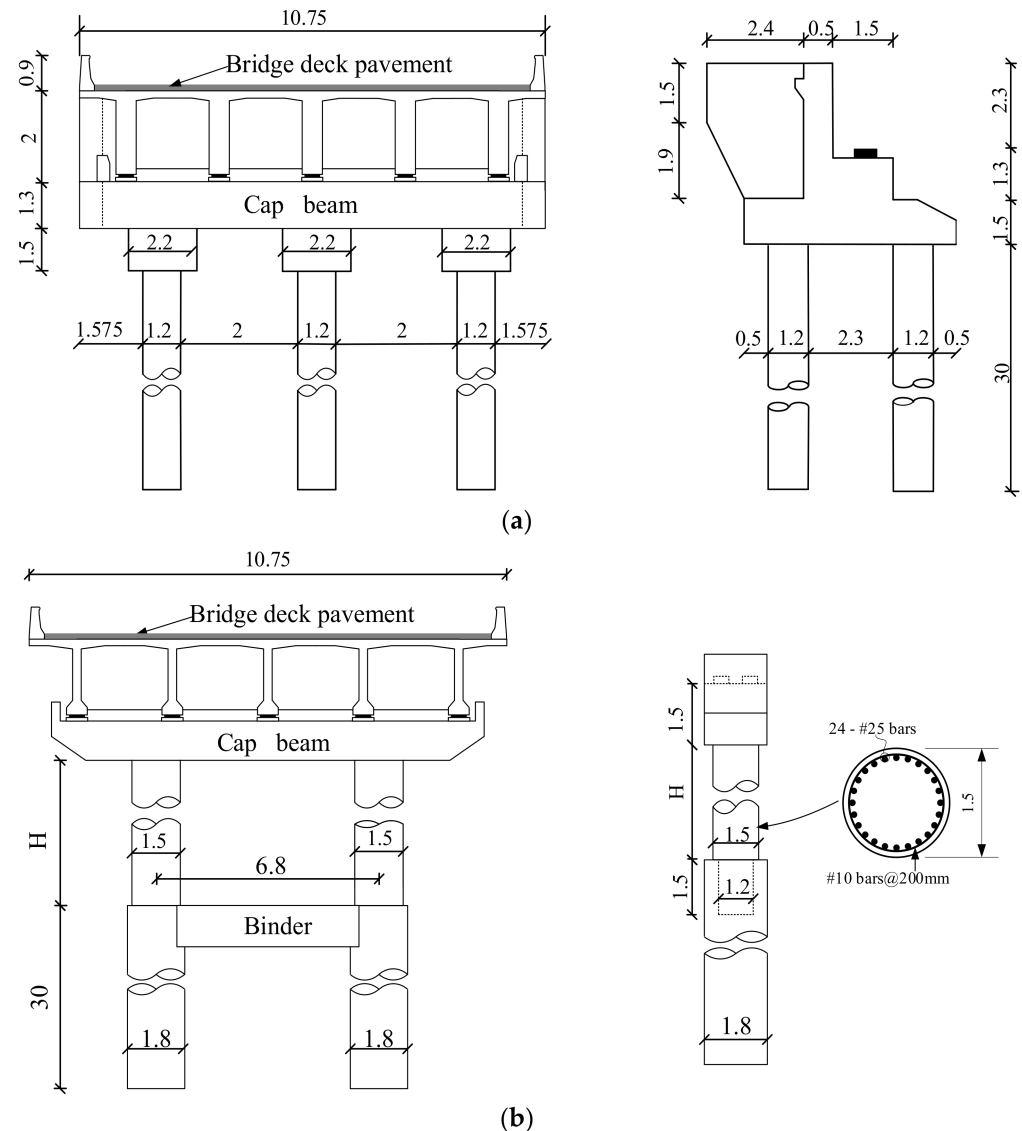


Figure 1. Bridge prototype (unit: m): (a) abutment layout; (b) pier layout.

2.2. Bridge Modeling

The nonlinear finite element models of the selected bridge are built using the open-source software OpenSees. It is acknowledged that decks are considerably stiff in compression with supporting abutments and columns. Therefore, the seismic response of bridges under earthquakes is dominated by the inelastic deformation of the columns and abutment backfill [22]. The deck remains elastic during earthquakes, so it was simulated by linear elastic beam elements (spline model), which provides low computational intensity and effectively represents the stiffness of the deck.

The pier columns were simulated with nonlinear beam-column elements. The cross-section of the bridge column was divided into unconfined concrete fiber and confined concrete fiber. The concrete fiber was simulated with the Kent-Scott-Park model, which does not account for the tensile strength of concrete when exposed to degraded linear unloading and reloading stiffness [23]. The reinforcement was simulated with the Giuffre-Menegotto-Pinto model, which could account for the two-way Bauschinger effect and the equivalent strengthening effect. Table 1 lists the parameters of the unconfined and confined concrete while Table 2 lists the parameters of rebar material.

Table 1. Parameters of Concrete Material.

Type	Compressive Strength f_c' (MPa)	Crushing Strength f_{cu} (MPa)	Strain at Peak Strength ϵ_0	Ultimate Strain ϵ_u
Unconfined concrete	28.00	5.60	0.0020	0.006
Confined concrete	31.96	6.39	0.0040	0.010

Table 2. Parameters of Rebar Material.

Type	Yield Strength F_y (MPa)	Initial Elastic Tangent E (Mpa)	Strain-Hardening Ratio
Rebar	400.0	206,000	0.01

Pot-sliding bearings and PTFE rubber bearings are commonly used in highway bridges in China, which will slip once the horizontal shear force to be transferred is greater than the friction between the contact surfaces. The load-displacement hysteretic relationship of the bearings was simulated by the ideal elastoplastic model.

Abutment Backwall Modeling

The geometry of a seat-type abutment is made up of two parts: a backwall and a breast wall. The backwall refers to the back of the seat and is a little higher than the main beam, while the breast wall, which is broader, generally extends from the backwall's bottom to the foundation's top. For the longitudinal abutment response in the current Caltrans seismic design criteria [24], the abutment is defined as a capacity-protected component, and the ideal bilinear force-deformation relationship is adopted to describe the abutment's behavior.

However, when bridges are subjected to earthquake loads, the impact between the backwall and deck may make the abutment suffer shear failure with a crack of approximately 45° at the juncture of the abutment [13]. Since it is much easier to fix the backwall than the breast wall, such a mode of failure is even recommended to use in seismic design. Considering that the reinforcement layout and failure mode of a seat-type abutment is similar to the reinforced concrete shear key, this paper adopts a simplified elastic-plastic model to consider the damaged backwall. The simplified model was obtained on the basis of a hysteresis rule for exterior shear keys proposed by Silva et al. [25]. Figure 2 shows the force-displacement skeleton curves of the linear elastic backwall and damaged backwall models. The models include the nonlinear force-displacement relationship of abutment backwall damage, which can more truly reflect the longitudinal seismic response of the bridge.

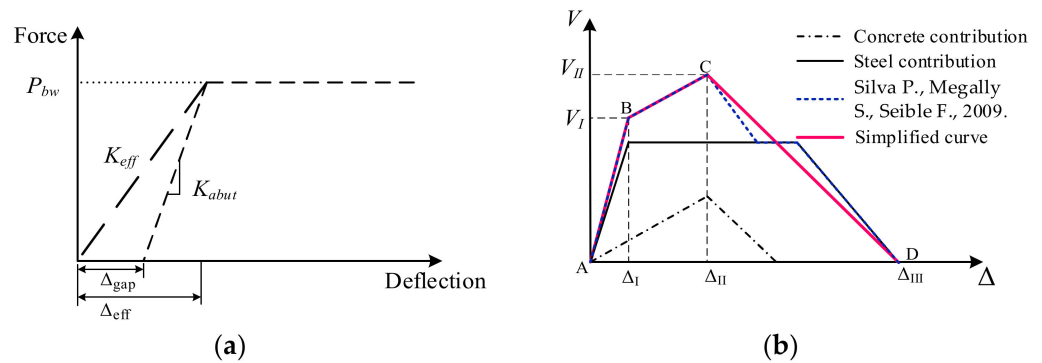


Figure 2. Force–displacement curve of backwall: (a) linear elastic backwall; (b) nonlinear backwall [25].

K_{abut} is the adjusted initial stiffness of the backwall of the seat-type abutment. K_{eff} is the effective abutment wall stiffness of the seat-type abutment accounting for the expansion hinge gaps. The simplified skeleton curve of the damaged backwall is divided into three sections: yield (AB line), hardening (BC line), and failure (CD line). The relationship between the shear force and displacement at three stages can be determined by Equations (1)–(4).

$$V_I = V_S + \frac{\Delta_{II}}{\Delta_{III}} V_C \quad (1)$$

$$V_{II} = V_C + V_S \quad (2)$$

$$V_C = 0.2 \sqrt{f'_c} B h \quad (3)$$

$$V_S = (A_s f_{ys} h + A_v f_{yv} d) / (h + a) \quad (4)$$

where V_S is the contribution of steel to the abutment's capacity; V_C is concrete's contribution to the abutment capacity; f'_c is the compressive strength of concrete; h is the vertical height of the cracked area of the backwall; B is the width of the abutment; a is the height of the loading point from the backwall's bottom; A_v and f_{yv} are the area and yield strength for vertical steel bars on the tension side, respectively; and A_s and f_{ys} are the area and yield strength for the horizontal stirrups at the upper edge of the cap beam. Δ_I is the displacement at the yielding point; Δ_{II} is the displacement at the hardening point; and Δ_{III} is the displacement where the shear key reinforcement fails. The values of various parameters are as follows: $V_S = 2680.83 \text{ kN}$; $V_C = 3769.39 \text{ kN}$; $\Delta_I = 0.00394 \text{ m}$; $\Delta_{II} = 0.0158 \text{ m}$; $\Delta_{III} = 0.039 \text{ m}$.

In addition, the modeling of abutment-soil-foundation-superstructure interactions is elaborated in the following Section 2.3. The finite element model of the entire bridge system is presented in Figure 3a. The fiber section, the stress-strain constitutive model of concrete and rebar, and the hysteresis model of pot-type bearings are exhibited in Figure 3c–e, respectively.

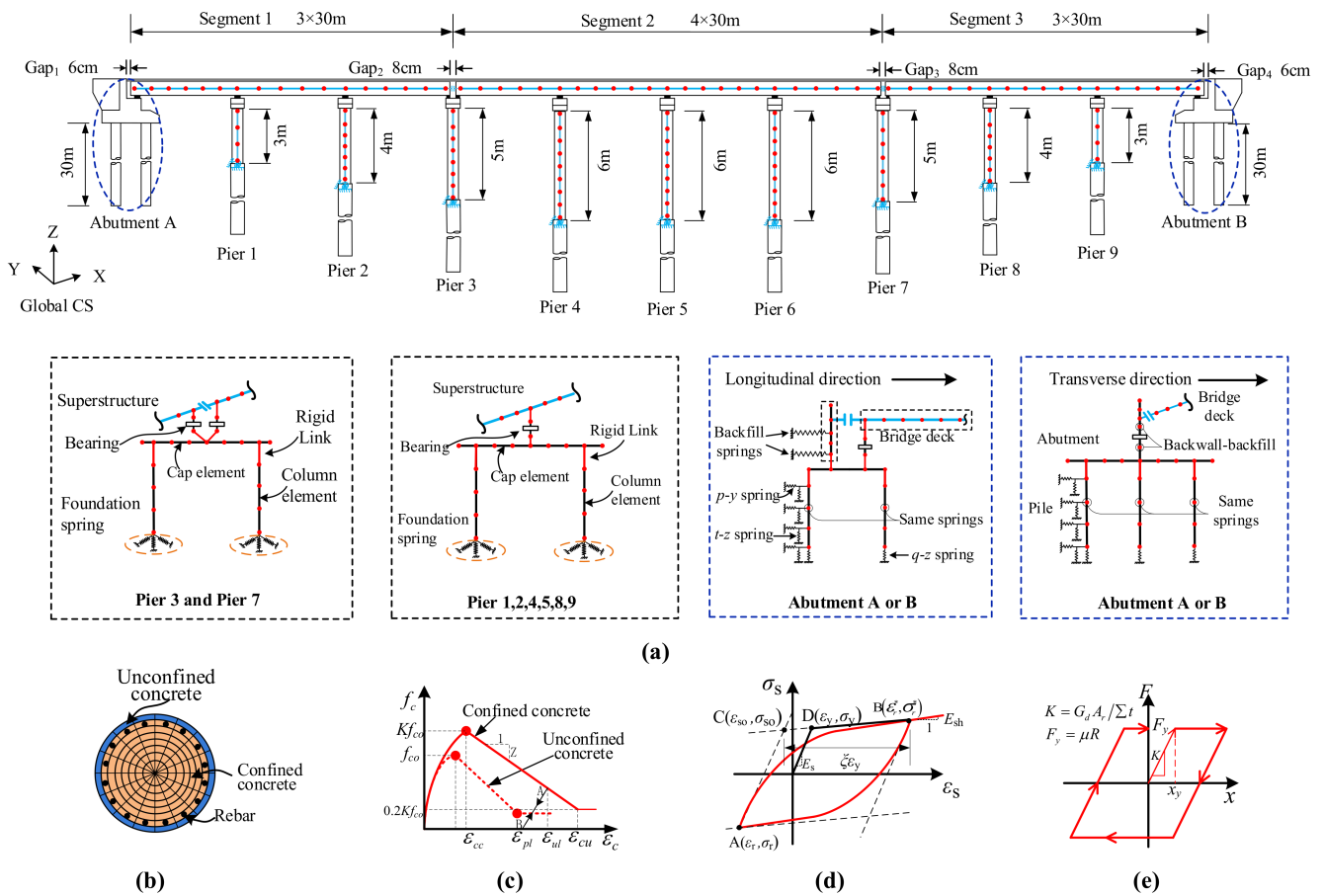


Figure 3. Numerical model and material constitution of the bridge: (a) numerical model; (b) fiber section; (c) concrete stress-strain constitutive model; (d) rebar stress-strain constitutive model; (e) hysteresis model of pot-type bearings.

2.3. Abutment-Soil-Foundation-Superstructure Interactions

2.3.1. Abutment-Backfill Interaction Modeling

The pounding between the beam and abutment occurs during earthquakes when their relative displacement exceeds the gap of the expansion joint. Then, the pounding force will be transmitted to the backfill and its foundation through the abutment, making passive resistance mobilized in the backfill. In order to determine the dynamic process of the passive earth pressure-deformation of the soil under earthquakes, the hyperbolic method proposed by Duncan et al. is used to attain the force-displacement relationship of the abutment-backfill system [26]. The hyperbolic force-displacement relationship is shown in Equation (5). It is assumed that once the backwall is destroyed, the backfill behind the backwall makes no difference to the bridge. For this purpose, two nonlinear springs are adopted to simulate the abutment-backfill interactions. Among them, the backwall-backfill spring automatically fails when the backwall is damaged, but the cap-backfill spring still works. This setting is conservative for the sliding displacement response.

$$P = y / \left(\frac{1}{K_{max}} + R_f \frac{y}{P_{ult}} \right) \tag{5}$$

where P is the passive earth pressure acting on the backwall; y is the horizontal deformation of the backfill; P_{ult} is the maximum passive earth pressure acting on the backwall; K_{max} is the initial stiffness; and R_f is the empirical coefficient, which takes a value between 0.75 and 0.95.

The initial stiffness K_{max} was solved according to an elastic method proposed by Douglas et al. [27], as shown in Figure 4a. Rectangle ABCD represents a flat plate in an elastic semi-infinite space, with uniform distribution force q acting on one side of the flat plate. It is assumed that the soil on the other side is an elastic medium, which could be characterized by Young's modulus and Poisson's ratio. Then, the mean displacement of four points, namely y_{ave} , can be solved. Finally, the stiffness of the rectangular plate-fill system, K_{max} , is calculated by Equation (6).

$$K_{max} = \frac{q \cdot b \cdot h}{y_{ave}} \quad (6)$$

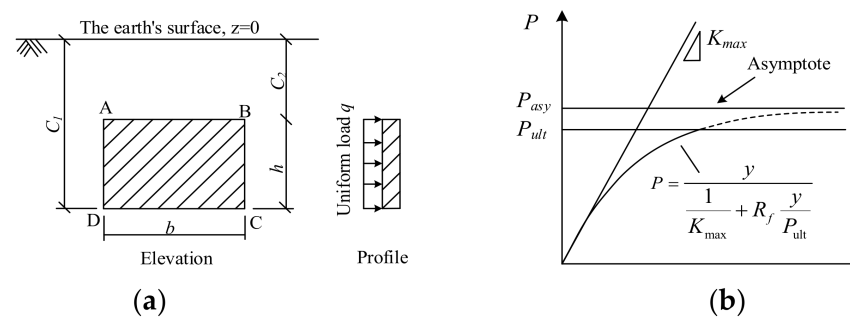


Figure 4. Abutment–backfill interaction modeling: (a) schematic diagram of the calculation of K_{max} ; (b) force–displacement relationship.

The calculation methods of the maximum passive earth pressure include the classical Coulomb theory, Rankine theory, the logarithmic spiral-slice method, etc. This paper adopts Rankine's earth pressure theory [28]. The maximum passive earth pressure acting on the backwall is calculated by Equation (7).

$$P_{ult} = \frac{1}{2} \gamma H^2 \tan^2 \left(45^\circ + \frac{\phi}{2} \right) \quad (7)$$

where γ is the weight of sand filling behind the abutment, ϕ is the internal friction angle of sandy soil, and H is the height of the backwall. The force-displacement curve of the abutment-backfill system calculated by the above method is shown in Figure 4b.

2.3.2. Pile–Soil Interaction Modeling

Owing to the sliding effect of the plate-type elastomeric pad bearings, a small seismic inertial force is transmitted to the pier and its pile foundation. It is not necessary to account for the pile-soil interactions at piers in the finite element model. To facilitate calculations and analysis, six-degrees-of-freedom springs were used to simulate the role of foundations acting on piers, and the tie beam at the pier bottom was ignored. It is noted that the equivalent stiffness of the springs was calculated through the M method.

The pile-soil interactions were modeled based on the nonlinear Winkler Foundation method. Abutment piles are simulated using the nonlinear fiber elements with a length of 1 m. The pile cap was simulated with the elastic beam-column elements.

The lateral soil's resistance on piles was modeled with nonlinear zero-length p - y springs. The nonlinearity of the p - y spring was considered by the PySimple1 material in OpenSees. The p - y model for clay was developed by the Matlock clay relationship [29], and the ultimate resistance for clay was determined by Equation (8).

$$P = \begin{cases} 3c + \gamma X + J \times c \times X/D & X < X_R \\ 9c & X \geq X_R \end{cases} \quad (8)$$

where c is the undrained shear strength for undisturbed clay samples, J is the nondimensional empirical constant with values from 0.25 to 0.5, γ is the effective unit weight of the soil, X is the depth below the surface of the soil, D is the average pile diameter, and X_R is the depth from the soil surface to the reduced resistance zone bottom.

The p - y model for sand was developed by the Parker and Reese sand relationship, which is recommended by API guidelines [30,31]. The ultimate resistance for sand was calculated by Equations (9)–(12).

$$P = A \times p_u \times \tanh \left[\frac{k \times H}{A \times p_u} \times y \right] \quad (9)$$

$$p_u = \min[p_{us}, p_{ud}] \quad (10)$$

where

$$p_{us} = (C_1 \times H + C_2 \times D) \times \gamma \times H \quad (11)$$

And

$$p_{ud} = C_3 \times D \times \gamma \times H \quad (12)$$

where A is the factor for cyclic loading; p_u is the ultimate bearing capacity at depth H ; k is the initial modulus of the subgrade reaction; C_1 , C_2 and C_3 are the coefficients obtained from API guidelines; γ is the effective soil weight; y is the lateral deflection of sandy soil; and H is the depth of sandy soil. The ultimate resistance for sand p_u results in a smaller value of p_{us} or p_{ud} ; p_{us} and p_{ud} are the ultimate soil-bearing capacity determined by shallow and deep depths, respectively.

The axial soil resistance acting on the pile's surface can be divided into two parts: axial adhesion between the pile and the surrounding soils and the end-bearing capacity at the pile's tip. Similarly, nonlinear zero-length t - z and q - z springs are adopted to represent the relationship between the axial soil resistance and soil deflection. The nonlinear behavior of the t - z and q - z springs is considered by the TzSimple1 and QzSimple1 materials in *OpenSees*, respectively. The t - z model for clay follows Reese and O'Neill's clay relationship, and the t - z model for sand follows Mosher's sand relationship [32,33]. The q - z model for clay follows the Reese and O'Neill clay relationship, and the q - z model for sand follows Vijayvergiya's sand relationship [34]. Figure 5a-f shows the values of the p - y , t - z and q - z models, respectively, in clay and sand.

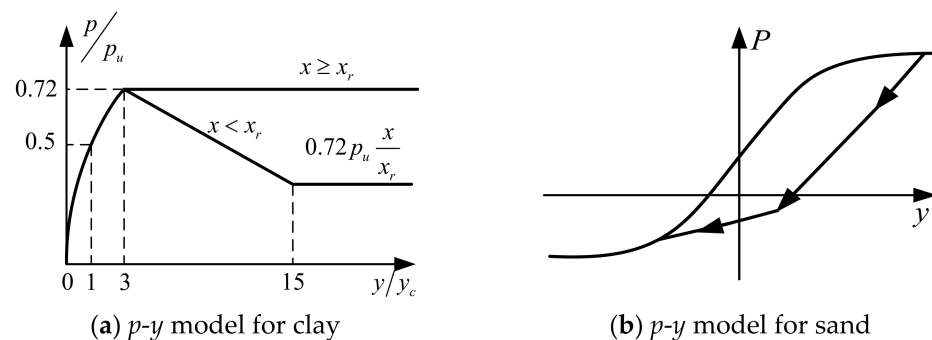


Figure 5. Cont.

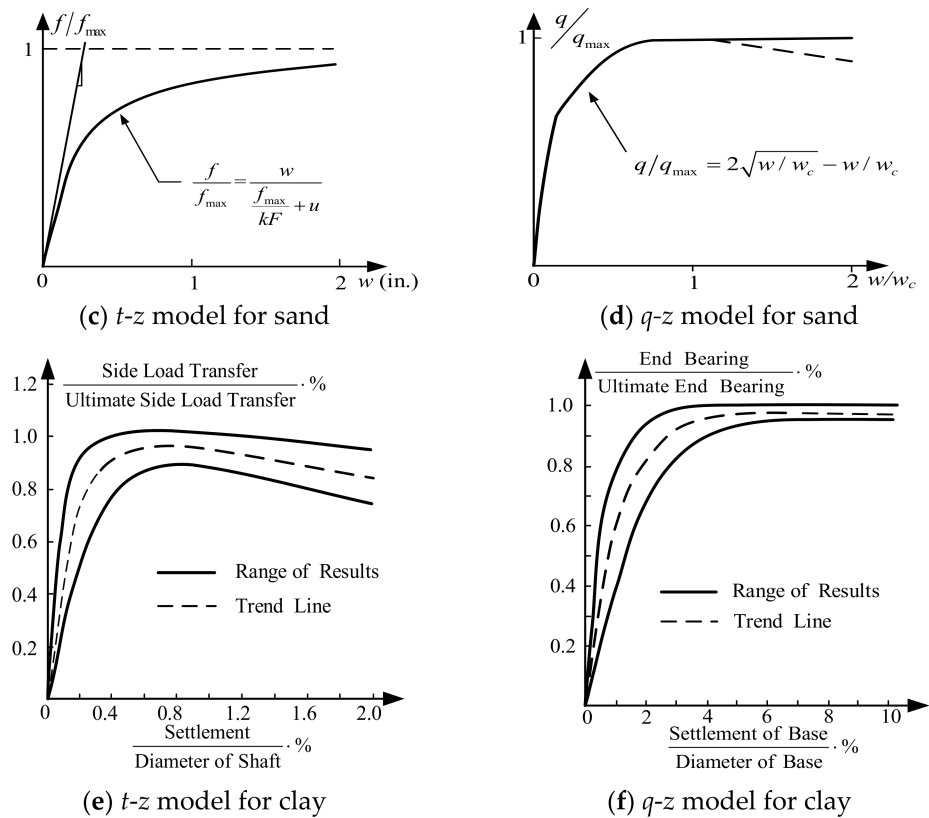


Figure 5. Pile-soil interaction models.

2.3.3. Pounding Modeling

The contact–element approach is widely used to model the impact between adjacent structures for its easy adaptability and relatively high efficiency [35]. There are mainly four types of contact element models used by scholars around the world: the linear spring model, the Hertz model, the Kelvin model, and the Hertz-damp model.

The Kelvin model (as shown in Figure 6) is adopted to model the pounding between adjacent structures. The Kelvin model and its contact force-displacement relationship are shown in Figures 6a,b, respectively. The pounding force F_p can be calculated with Equations (13)–(15).

$$F_p = \begin{cases} K_P \times (D - d_0) + c_k \dot{D} & D > d_0 \\ 0 & D \leq d_0 \end{cases} \quad (13)$$

$$c_k = 2\zeta \sqrt{K_P \frac{m_1 m_2}{m_1 + m_2}} \quad (14)$$

$$\zeta = -\frac{\ln e}{\sqrt{\pi^2 + (\ln e)^2}} \quad (15)$$

where D and d_0 are the relative displacement and the initial gap between adjacent structures, respectively. The stiffness of the pounding element, $K_P = 1.23 \times 10^6$ kN/m, is calculated as the average axial stiffness of the middle segment; the initial gap at the abutment expansion joint is $d_0 = 0.06$ m, and the initial gap at pier (P₃, P₇) expansion joint is $d_0 = 0.08$ m. c_k is the damping between two masses m_1 and m_2 . ζ is the damping ratio, which is relevant to a coefficient of restitution e , and e is 0.65 for reinforced concrete structures [36].

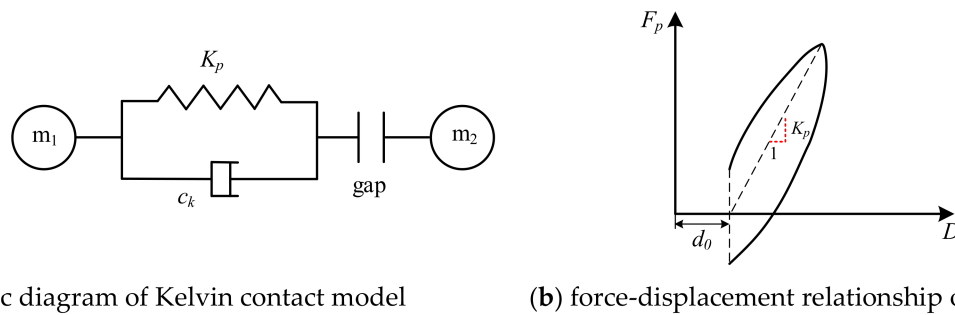


Figure 6. Kelvin model.

There were 1980 nodes and 1780 elements in the whole bridge model. Superstructure decks, abutment cap beams and pile caps were modeled using elastic beam-column elements because there is a tendency for them to remain elastic during seismic events. Zero-length elements with different material properties were utilized to simulate the bearings, pile-soil-structural interactions, and pounding effect.

2.4. Selection of the Ground Motions

An adequate number of ground motions is necessary to obtain a realistic prediction of seismic responses for bridges. For this study, it is of great importance to obtain statistically stable average values of the structural response to draw reasonable conclusions about the global responses. The consensus that seven or more spectrum-compatible time histories are eligible for averaging was reached. For this reason, thirty typical ground motion records downloaded from the strong motion database in PEER were selected as inputs in the numerical analyses. The PGA (peak ground acceleration) ranged from 0.10 to 0.24 g. The moment magnitude ranged from 6.46 to 7.62. The range of distance from the epicenter was from 30.56 to 58.28 km. The selected bridge was located in a class II ground motion site in China, and its seismic fortification intensity was IX degree [37]. The design acceleration response spectra of the bridge site are shown in Figure 7. The mean spectra of the selected earthquake waves matched the design spectra well. Hence, all thirty records were scaled to a peak ground acceleration of 0.4 g. Since this study focuses on the longitudinal motion of the bridge girders, the vertical and horizontal components (in the transverse bridge direction) of ground motions were not accounted for. The characteristics of input ground motions selected for this research are presented in Table 3.

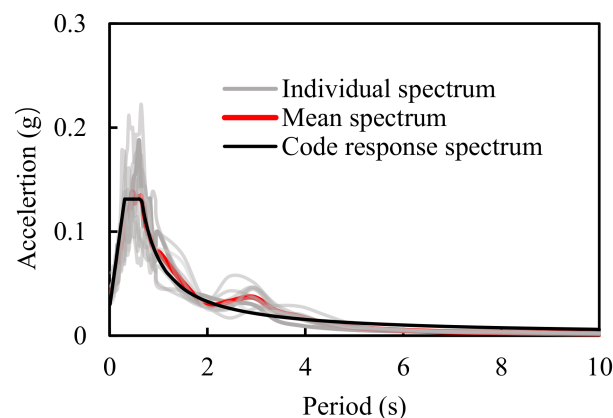


Figure 7. Acceleration response spectra of selected earthquake motion records.

Table 3. Characteristics of Input Motions.

ID	Earthquake	Station	Distance (km)	PGA (g)
1	Borrego Mountain	El Centro Array #9	45.12	0.13
2	San Fernando	Whittier Narrows Dam	39.45	0.10
3	Imperial Valley-06	Niland Fire Station	35.64	0.11
4	Coalinga-01	Parkfield-Fault Zone 2	37.92	0.12
5	Loma Prieta	Dumbarton Bridge West End FF	35.31	0.13
6	Loma Prieta	Palo Alto-1900 Embarc.	30.56	0.21
7	Big Bear-01	San Bernardino-2nd& Arrowhead	33.56	0.11
8	Northridge-01	Camarillo	34.78	0.12
9	Taiwan SMART1C00	SMART1 C00	56.01	0.15
10	Taiwan SMART1C00	SMART1 E01	53.31	0.16
11	Taiwan SMART1C00	SMART1 E01	53.31	0.19
12	Taiwan SMART1C00	SMART1 I01	56.18	0.14
13	Taiwan SMART1C00	SMART1 M01	56.87	0.14
14	Taiwan SMART1C00	SMART1 M07	55.11	0.16
15	Taiwan SMART1C00	SMART1 M07	55.11	0.16
16	Taiwan SMART1C00	SMART1 O01	57.9	0.17
17	Taiwan SMART1C00	SMART1 O02	57.13	0.16
18	Taiwan SMART1C00	SMART1 O02	57.13	0.24
19	Taiwan SMART1C00	SMART1 O12	58	0.16
20	Cape Mendocino	Eureka-Myrtle & West	40.23	0.15
21	Cape Mendocino	Eureka-Myrtle & West	40.23	0.18
22	Landers	Indio-Coachella Canal	54.25	0.10
23	Landers	Indio-Coachella Canal	54.25	0.11
24	Kocaeli Turkey	Atakoy	56.49	0.10
25	Kocaeli Turkey	Zeytinburnu	51.98	0.12
26	Kocaeli_Turkey	Zeytinburnu	51.98	0.11
27	Chi-Chi_Taiwan	CHY015	38.13	0.15
28	Chi-Chi_Taiwan	CHY015	38.13	0.14
29	Chi-Chi_Taiwan	CHY088	37.48	0.21
30	Chi-Chi_Taiwan	CHY088	37.48	0.15

3. Results and Discussion

In order to analyze the effect of the abutment backwall on the seismic performance of multi-span bridges, two bridge models with different abutment behaviors were established based on the bridge configurations and named Model I and Model II, respectively. Model I assumes that the abutment backwall is a linear elastic component with sufficient yield strength that remains elastic during a seismic event. On the other hand, Model II assumes that the abutment backwall is a sacrificial component considering its failure mechanism, which is calculated according to Equations (1)–(4). The peak and mean responses of the bridge under thirty ground motions are presented, and the time history responses are adopted to specifically show how the abutment damage influences the seismic performance of the bridge.

3.1. Pounding Force Response

Figure 8a presents the peak pounding force at gap₁ for the bridge models under thirty ground motions. It can be found from Section 3.5 that the bridge with a sacrificial abutment backwall (Model II) induces a much smaller pounding force response than the bridge with a linear elastic abutment backwall (Model I). Figure 8b exhibits the mean pounding force at four gaps for the bridge models, respectively. It is clear that the mean pounding force at gap₁ between Segment 1 and abutment A is reduced from 9.86×10^3 kN (Model I) to 6.68×10^3 kN (Model II), with a decrease of 32.2%, and the mean pounding force between Segment 3 and abutment B is reduced from $9.12 \text{ MN} \times 10^3$ kN to 6.43×10^3 kN, with a decrease of 29.5%. The mean pounding force at gap₂ between Segment 1 and Segment 2 is reduced from 14.80×10^3 kN (Model I) to 7.96×10^3 kN (Model II), with a decrease of 46.2%, and the mean pounding force at gap₃ between Segment 2 and Segment 3 is reduced from 14.33×10^3 kN to 7.77×10^3 kN, with a decrease of 45.8%, which illustrates that it

is of great benefit for the bridge to equip a sacrificial abutment backwall to mitigate the pounding between the abutment and bridge decks or adjacent decks.

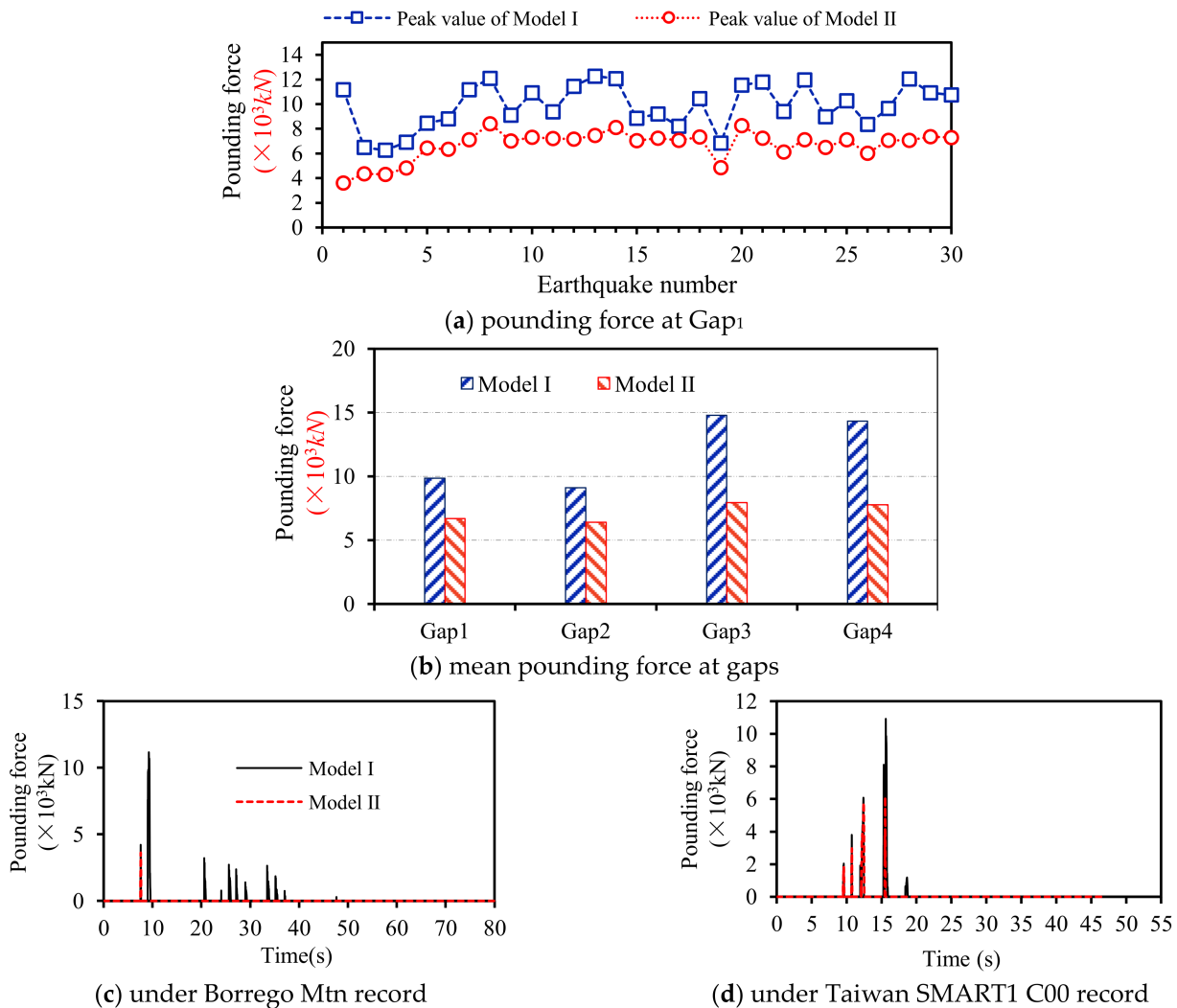


Figure 8. Pounding force response.

Figure 8c show the time histories of pounding force for the bridge models excited by the Borrego Mountain and Taiwan SMART1 C00 records, respectively. It is evident that the seismic response of the bridge is apparently affected when considering the abutment damage: the peak pounding force between the main beam and abutment A significantly decreases, and the number of poundings is also reduced.

3.2. Displacement Response

Figure 9a presents the mean displacement response for the bridge models. It can be found from Figure 9a that the mean deck displacement has an increasing trend when considering the abutment damage. To be specific, the mean longitudinal displacement of Segment 1 increases from 17.6 cm to 21.2 cm, Segment 2 from 18.6 cm to 22.7 cm, and Segment 3 from 17.6 cm to 21.8 cm, with increases of 20.4%, 22.1% and 23.5%, respectively.

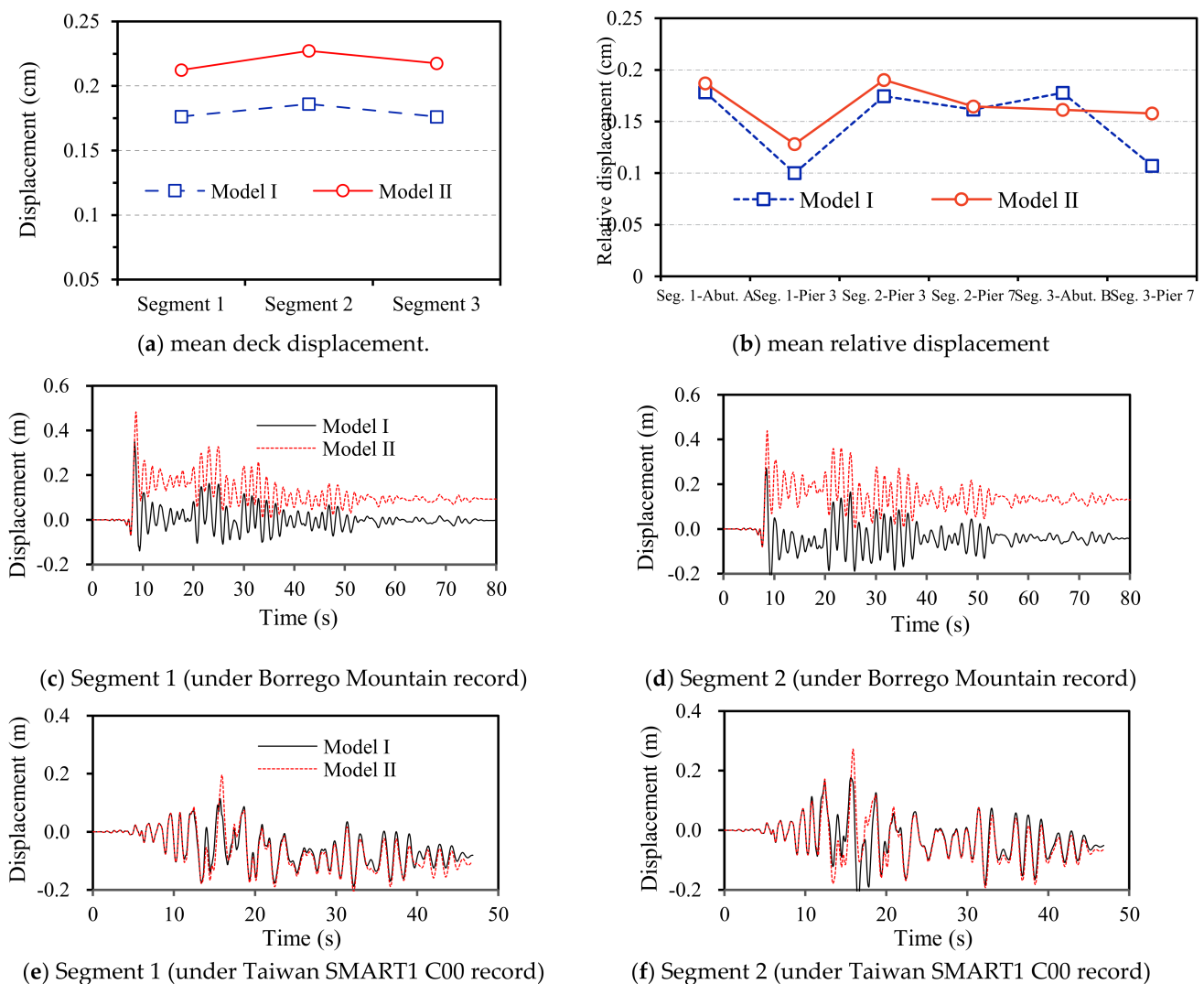


Figure 9. Displacement responses.

Figure 9b shows the mean relative displacement of the three-segment bridge model. It can be seen that there is no obvious rule to follow for the relative displacement between the main beam on the side and the respective abutment, but the mean relative displacements between Segment 2 and No. 3 or No. 7 pier are slightly increased, with increases of 9.0% and 1.9%, respectively. It also manifests that the damage of the abutment backwall has little influence on the risk of a girder falling at the abutment but greatly increases the risk of a girder falling at the No. 3 or No. 7 pier.

From the time history of longitudinal deck displacement, as seen in Figure 9c–f, it can be observed that the longitudinal deck displacement is apparently affected when considering the abutment damage (Model II), resulting in a larger peak displacement and residual displacement than the bridge model with a linear elastic abutment (Model I). The bridge deck moved toward abutment B and had a positive residual displacement under the Borrego Mountain record, while the bridge deck moved toward abutment A and had a negative residual displacement under the Taiwan SMART1C00 record. This phenomenon shows that the specific offset to which side depends on the input ground motion excitation.

3.3. Abutment Backwall Response

The peak shear force at abutment A at the bottom of the bridge models is shown in Figure 10a. It can be noticed that the shear force at the backwall's bottom has a greatly

decreasing trend when considering the damage to the abutment. In addition, the peak shear force in Model II is mostly about $6 \times 10^3 \text{ kN}$, which is very close to the ultimate shear capacity at the backwall's bottom ($6.13 \times 10^3 \text{ kN}$) calculated by Equation (2). Hence, the abutment reaches shear failure when excited by most selected ground motions.

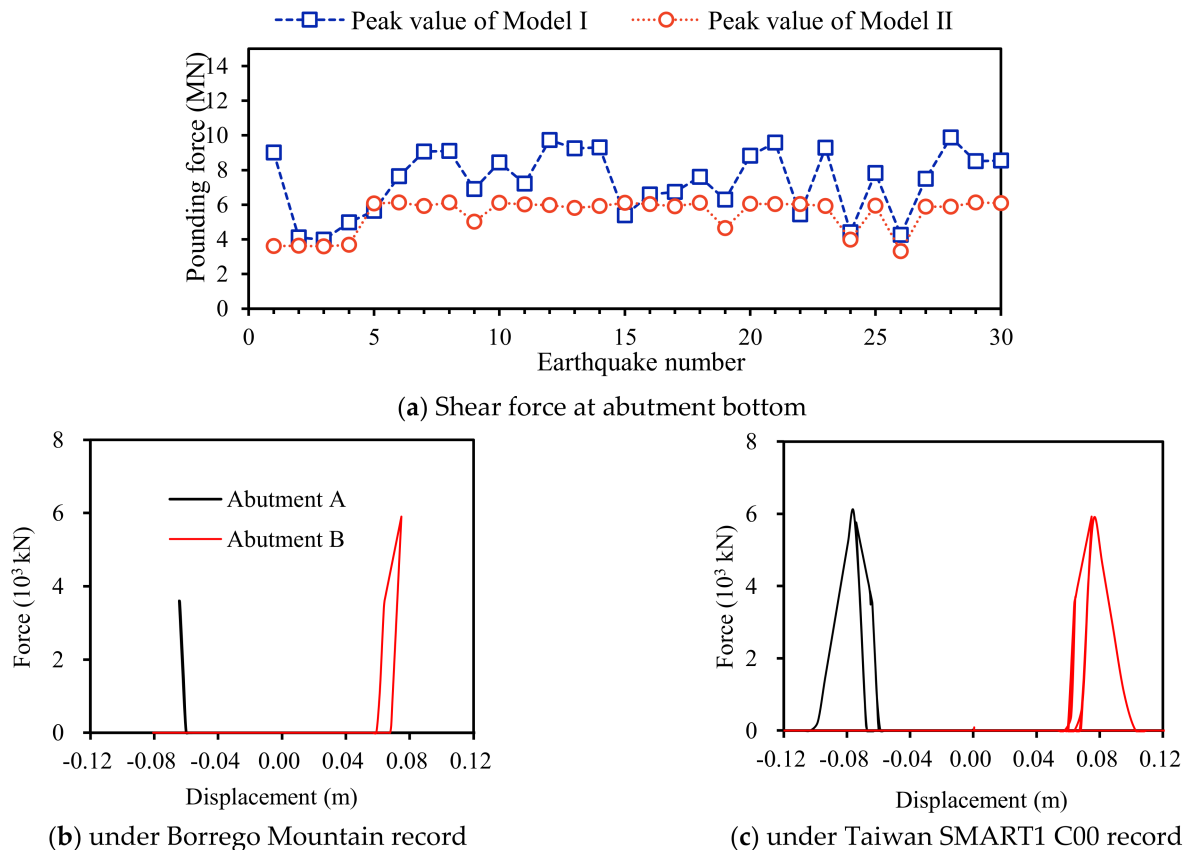


Figure 10. Abutment backwall response.

The hysteretic curves of the force-displacement of the abutment backwall for Model II under the Borrego Mountain and Taiwan SMART1 C00 records are shown in Figure 10b. It is noticed that severe plastic deformation is generated at the abutment backwall due to the huge pounding force, which further reflects that damage occurred to the abutment.

3.4. Abutment Backfill Response

Figure 11a-d shows the passive earth pressure-deformation hysteretic curve of the backfill for the two models under the Borrego Mountain and Taiwan SMART1 C00 record, respectively. It is found that for Model I, the passive earth pressure-deformation hysteresis curve of the backfill is full, behaving with obvious nonlinear characteristics; for Model II, the passive earth pressure and deformation of the abutment backfill are small, and the backfill remains elastic and even does not undergo plastic deformation.

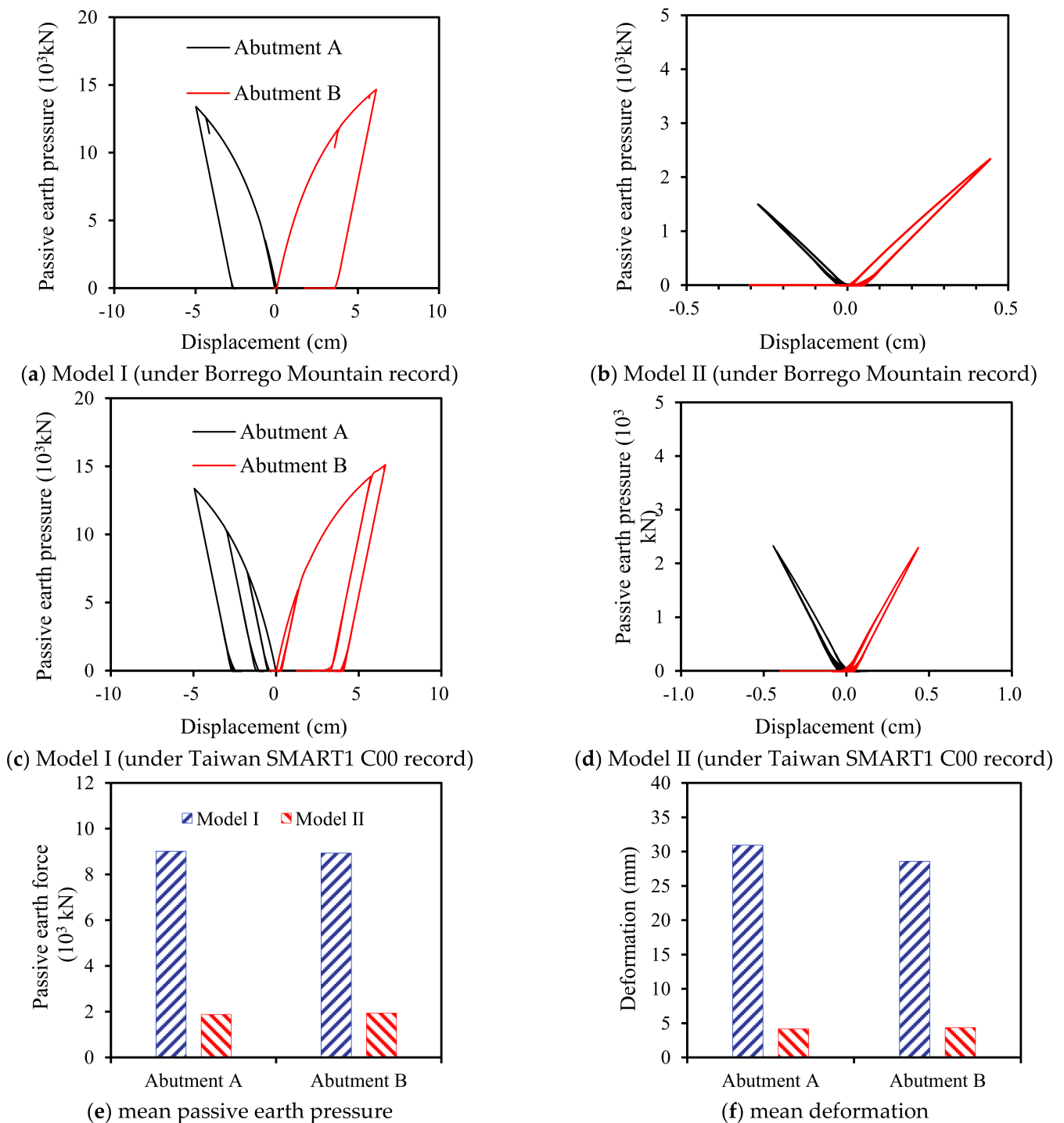


Figure 11. Backfill response.

Figure 11e,f shows the mean passive earth pressure and deformation of the backfill for the two models. It is apparent that the mean passive earth pressure and deformation has a decreasing trend if the backwall is sacrificial (Model II) rather than linear elastic (Model I). This is because the superstructure transmits a large amount of seismic inertial force to the abutment through pounding when the backwall is a linear elastic member, and the backwall simultaneously transmits part of the seismic inertial force to the backfill. Therefore, the passive earth pressure and deformation of the abutment backwall-backfill system is relatively large, but when the abutment is designed as a sacrificial member in the analysis

model, the pounding force probably causes the backwall to be destroyed. Then, the loss of the restraint of the abutment on the superstructure will reduce the rigidity of the structural system, making the seismic inertia force of the superstructure smaller. Hence, the passive earth pressure of the backwall-backfill system and deformation is significantly reduced.

3.5. Abutment Pile Response

In terms of the selected bridge, the pounding makes the abutment lean back when pounding between the abutment and deck occurs. As shown in Figure 12, the axial force response of front and rear row piles is quite different: the seismic axial force of the front-row piles is a tensile force, while this force is compressive for the rear-row piles. Furthermore, rear-row piles have compression-bending components, while front-row piles are likely to become tension-bending components under a combination of seismic and dead load. Since the axial force has a greater influence on the bending bearing capacity of the member bar, this section will focus on the axial force and bending moment response for the pile foundation at its abutments.

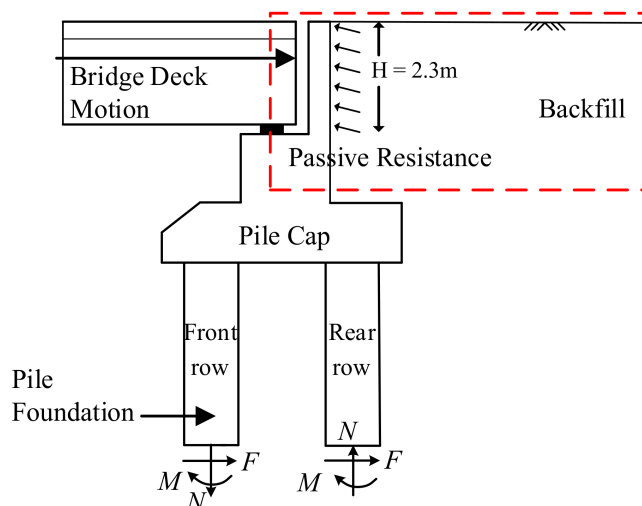
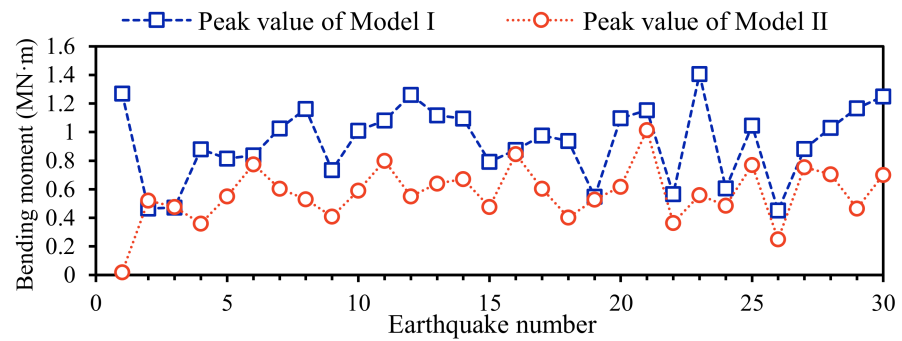
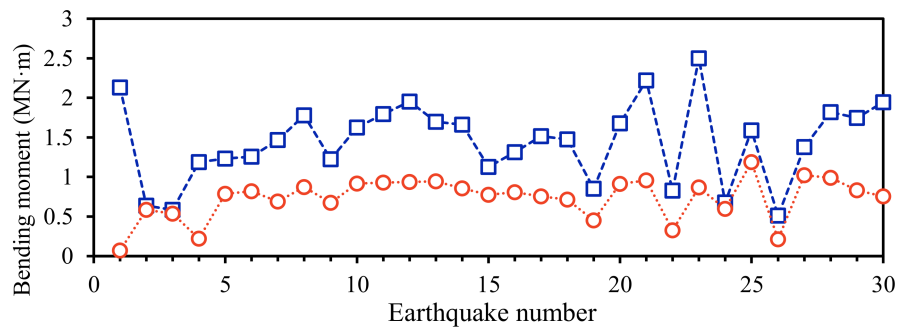


Figure 12. Force on abutment during pounding.

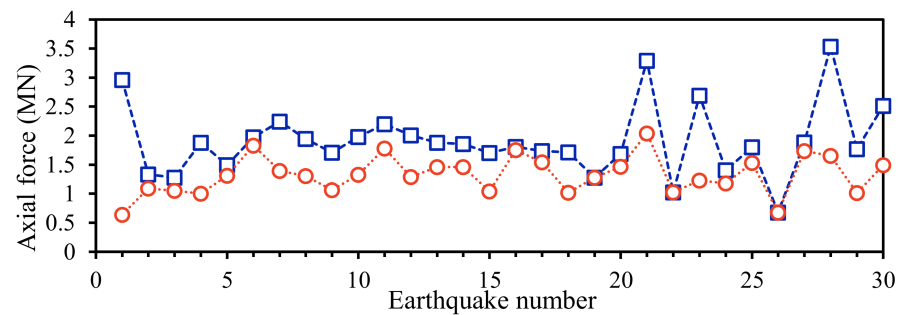
Figure 13a–d compares the peak value of the bending moment and axial force of abutment A piles for the bridge models under thirty ground motions. It is observed that the bridge with sacrificial abutments has a much smaller peak bending moment and axial force than that of the bridge with linear elastic abutments during a seismic event. Figure 13e,f shows the mean bending moments and axial forces of abutment A piles for the bridge models. As shown when ignoring the abutment damage, the axial force and bending moment of the abutment A pile are significantly increased. Specifically, the mean bending moment and axial force of the front row piles increase by 64.4% and 44.2%, respectively; the mean bending moment and axial force of the rear row piles increase by 97.2% and 93.0%, respectively. This means that the transmission of the seismic force of the main beam to the foundation through the abutment is effectively weakened due to the damage to the abutment under strong earthquakes, avoiding the risk of damage to the abutment's pile foundation.



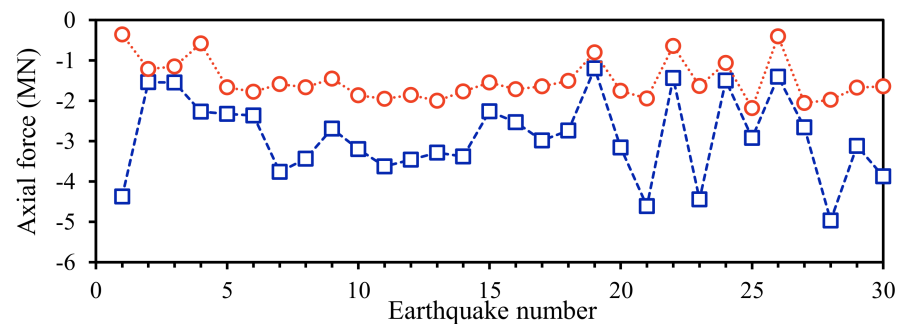
(a) front-row piles



(b) rear-row piles



(c) front-row piles



(d) rear-row piles

Figure 13. Cont.

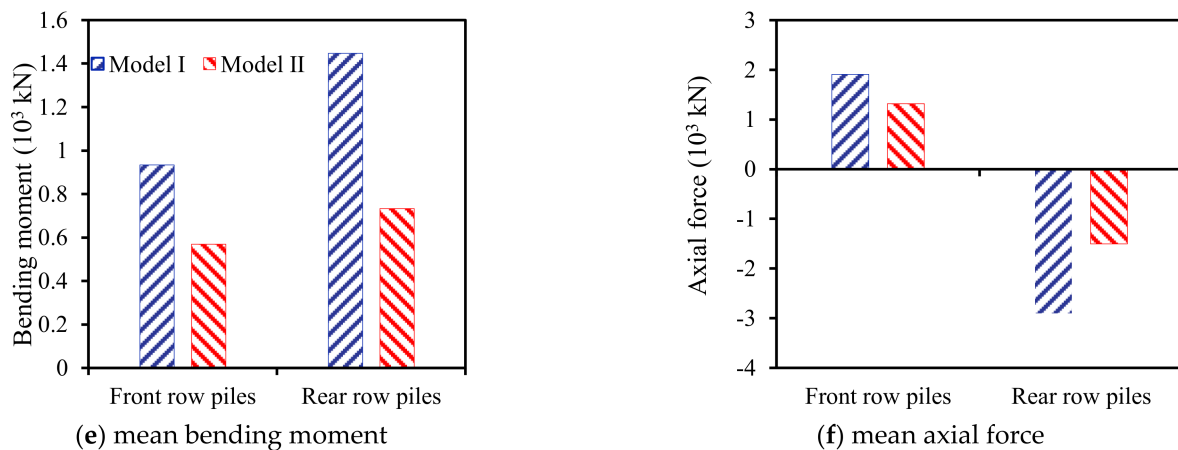


Figure 13. Bending moment and axial force response.

It is observed that the axial force of the front-row piles is much smaller than that of the rear-row piles owing to the interaction between the beam and the abutment. This is because the seismic axial force of the front row piles is a tensile force, while the seismic axial force of the rear row piles involves pressure. After the constant load axial force is combined, the value of the axial force of the front-row piles becomes smaller, and the value of the axial force of the rear-row piles becomes larger. Beyond that, the front-row piles subjected to tension are more likely to be damaged than the rear-row piles because the pile foundation has poor tensile performance.

Figure 14a,b exhibits the envelope of the bending moment, shear force and axial force of abutment A piles for the bridge models under the Borrego Mountain record. It indicates that the bending moment, shear force and axial force of the abutment A pile in each section are significantly reduced, which illustrates that the failure of the abutment is favorable to the abutment's foundation. In addition, the maximum bending moment and shear force appear at the pile's top section, while the maximum axial force appears near the -2 m section of the pile foundation.

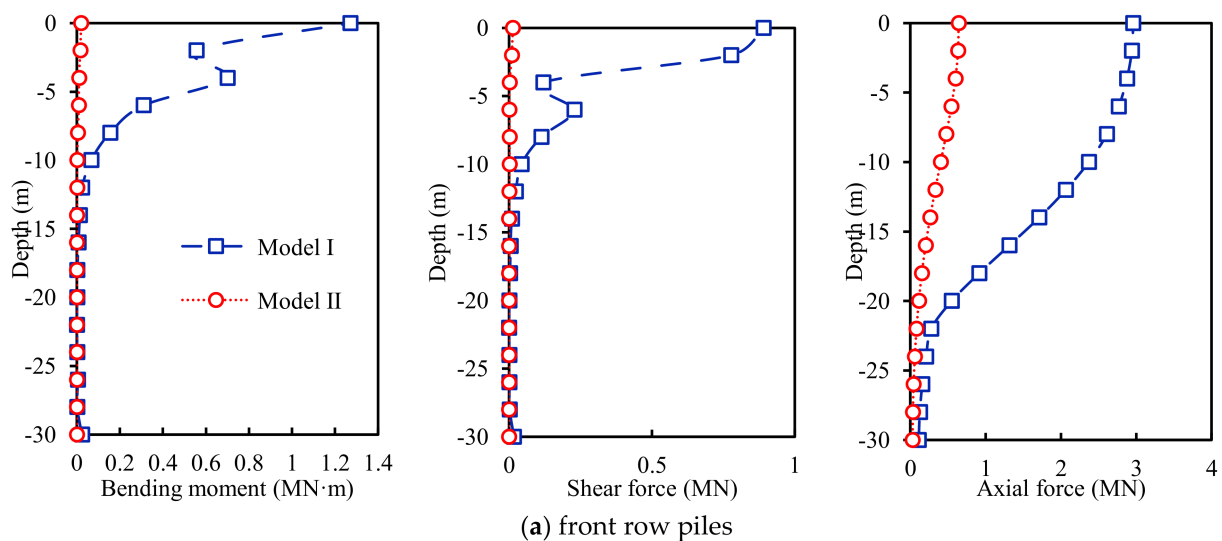


Figure 14. Cont.

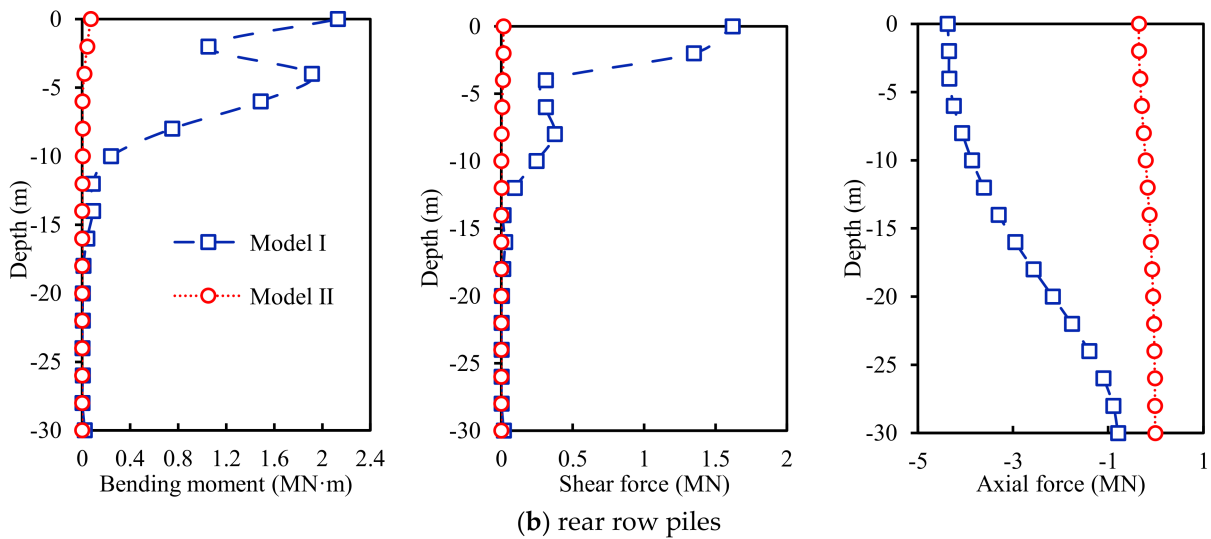


Figure 14. Envelope of bending moment, shear force and axial force (under Borrego Mountain record).

The force-displacement curve of p - y springs around the pile's top is presented in Figure 15. Similarly, it is found that the plastic deformation of the soil around the pile for the bridge with a sacrificial abutment obviously decreases and nearly disappears under strong earthquakes, compared with the bridge with a linear elastic abutment. As shown in Figure 14, for model I, the force-displacement hysteresis curve is full, and the nonlinear deformation is obvious, which means that the soil is seriously damaged; for model II, the bending moment and shear and axial force responses of the abutment foundation are small. Thus, the soil around the pile does not have much deformation, and it is still in an elastic state. This result implies that a sacrificial abutment design for bridges could alleviate the pounding between the beam and the abutment and then weaken the seismic response of the abutment's foundation. By contrast, the seismic response of bridges is intensified when the abutment backwall is designed as a linear elastic component.

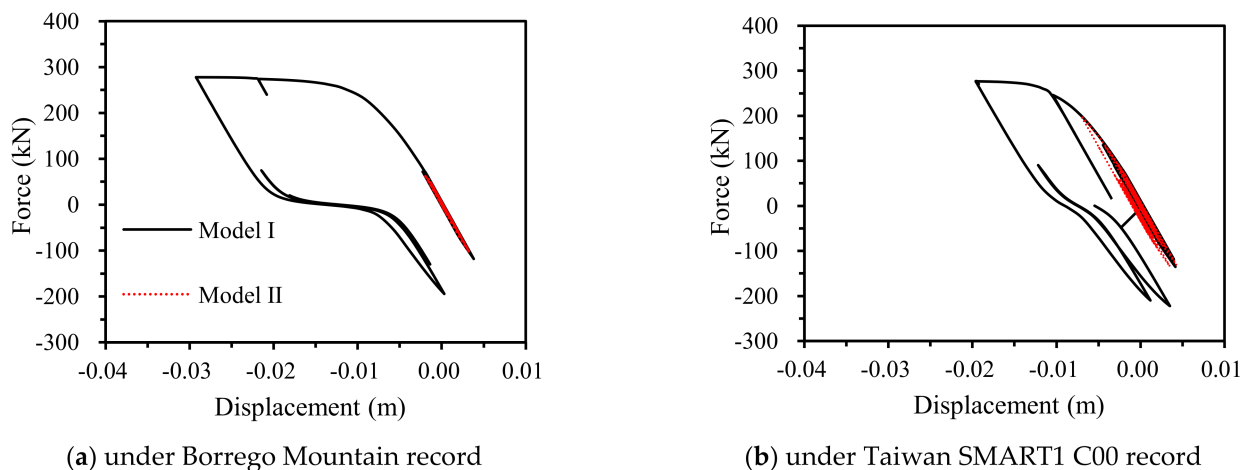


Figure 15. Force-displacement relation of p - y springs around pile top.

4. Summary and Conclusions

This study investigates the effect of longitudinal pounding and the abutment behavior of a typical highway bridge with seat-type abutments subjected to a strong earthquake. Three-dimensional finite element models of this multi-span bridge were developed, incorporating abutment-backfill interactions, soil-pile interactions, the pounding effect, the nonlinearity of the columns, and so forth. The seismic performance of multi-span bridges

with two different types of abutment behavior were evaluated through nonlinear time history analyses. Conclusions and suggestions are summarized as follows:

1. Pounding between the abutment back and the bridge deck could lead to the shear failure of the bridge abutments and the strength loss of the abutment backfill during a fierce seismic event. What is worse, the unseating of a girder may happen due to excessive deck displacement resulting from the failure of the abutment and backfill.
2. If the abutment backwall is designed as a linear elastic component with sufficient yield strength, the huge pounding force will be transmitted to the abutment's pile foundation through the abutment backwall, which can easily cause the abutment pile to suffer shear or bending failure or other serious damage.
3. If the abutment backwall is designed as a sacrificial component, it can effectively prevent the huge impact force from being transmitted to the abutment's pile foundation and protect the abutment's pile foundation from damage, but it is likely to make the beam body suffer a large displacement and cause the unseating of girders.
4. When the abutment backwall is designed as a sacrificial member, it is of great importance to select the right yield strength for the abutment backwall to achieve the balance of force and displacement, and a collapse-proof system should be employed to prevent the unseating of girders. The reasonable strength of the abutment backwall is sought to reduce the degree of damage to the abutment's pile foundation while not excessively increasing the displacement of the main beam. This is a further refinement of the existing specifications.

Author Contributions: Conceptualization, Y.D. and S.G.; methodology, S.G.; software, S.G.; validation, Y.D., S.G. and F.L.; formal analysis, S.G.; investigation, F.L.; resources, Y.D.; data curation, S.G.; writing—original draft preparation, S.G.; writing—review and editing, Y.D.; visualization, F.L.; supervision, Y.D.; project administration, Y.D.; funding acquisition, Y.D. All authors have read and agreed to the published version of the manuscript.

Funding: This research was funded by the National Natural Science Foundation of China Grants Number 51678459.

Institutional Review Board Statement: Not applicable.

Informed Consent Statement: Not applicable.

Data Availability Statement: The data are not publicly available due to privacy.

Conflicts of Interest: The authors declare no conflict of interest.

References

1. Loh, C.H.; Lee, Z.K.; Wu, T.C.; Peng, S.Y. Ground motion characteristics of the Chi-Chi earthquake of 21 September 1999. *Earthq. Eng. Struct. Dyn.* **2015**, *29*, 867–897. [[CrossRef](#)]
2. Chouw, N.; Hao, H. Pounding damage to buildings and bridges in the 22 February 2011 Christchurch earthquake. *Int. J. Prot. Struct.* **2012**, *3*, 123–139. [[CrossRef](#)]
3. Li, J.; Peng, T.; Xu, Y. Damage investigation of girder bridges under the Wenchuan earthquake and corresponding seismic design recommendations. *Earthq. Eng. Eng. Vib.* **2008**, *7*, 337–344. [[CrossRef](#)]
4. Abbasi, M.; Zakeri, B.; Amiri, G.G. Probabilistic Seismic Assessment of Multi-frame Concrete Box-girder Bridges with Unequal-height Piers. *J. Perform. Constr. Facil.* **2016**, *30*, 04015016. [[CrossRef](#)]
5. Wilson, P.; Elgamal, A. Full-scale shake table investigation of bridge abutment lateral earth pressure. *Bull. N. Z. Natl. Soc. Earthq. Eng.* **2009**, *42*, 39–46. [[CrossRef](#)]
6. Saiidi, M.; Vosooghi, A.; Nelson, R. Shake table studies of a four-span reinforced concrete bridge. *J. Struct. Eng.* **2013**, *139*, 1352–1361. [[CrossRef](#)]
7. Fiorentino, G.; Cengiz, C.; De Luca, F.; Mylonakis, G.; Karamitros, D.; Dietz, M.; Dihoru, L.; Lavorato, D.; Briseghella, B.; Isakovic, T.; et al. Integral abutment bridges: Investigation of seismic soil–structure interaction effects by shaking table testing. *Earthq. Eng. Struct. Dyn.* **2021**, *50*, 1517–1538. [[CrossRef](#)]
8. Aviram, A.; Mackie, K.R.; Stojadinovic, B. Effect of abutment modelling on the seismic response of bridge structures. *Earthq. Eng. Eng. Vib.* **2008**, *7*, 395–402. [[CrossRef](#)]
9. Shamsabadi, A.; Xu, S.Y.; Taciroglu, E. A generalized log–spiral–Rankine limit equilibrium model for seismic earth pressure analysis. *Soil Dyn. Earthq. Eng.* **2013**, *49*, 197–209. [[CrossRef](#)]

10. Erhan, S.; Dicleli, M. Comparative assessment of the seismic performance of integral and conventional bridges with respect to the differences at the abutments. *Bull. Earthq. Eng.* **2015**, *13*, 653–677. [[CrossRef](#)]
11. Shamsabadi, A.; Kapuskar, M. Nonlinear soil–abutment–foundation–structure interaction analysis of skewed bridges subjected to near-field ground motions. *Transp. Res. Rec.* **2018**, *2202*, 192–205. [[CrossRef](#)]
12. Luo, J.; Fahnestock, L.A.; Kozak, D.L.; LaFave, J.M. Seismic analysis incorporating detailed structure–abutment–foundation interaction for quasi-isolated highway bridges. *Struct. Infrastruct. Eng.* **2017**, *13*, 581–603. [[CrossRef](#)]
13. Thomaidis, I.M.; Kappos, A.J.; Camara, A. Dynamics and seismic performance of rocking bridges accounting for the abutment–backfill contribution. *Earthq. Eng. Struct. Dyn.* **2020**, *49*, 1161–1179. [[CrossRef](#)]
14. Liu, J.; He, J.; Ding, B.Y. 3D finite element analysis on bearing capacity characteristics of the composite ground. In *Ground Modification and Seismic Mitigation*; American Society of Civil Engineers: Reston, VA, USA, 2006; pp. 305–312.
15. Basack, S.; Nimbalkar, S. Numerical solution of single pile subjected to torsional cyclic load. *Int. J. Geomech.* **2017**, *17*, 04017016. [[CrossRef](#)]
16. Li, X.; Wan, J.; Zhao, H.; Liu, S. Three-dimensional analysis of nonlinear pile–soil interaction responses using 3D Pile Element Model. *Int. J. Geomech.* **2021**, *21*, 04021129. [[CrossRef](#)]
17. Phanikanth, V.S.; Choudhury, D.; Reddy, G.R. Behavior of single pile in liquefied deposits during earthquakes. *Int. J. Geomech.* **2013**, *13*, 454–462. [[CrossRef](#)]
18. Wang, X.; Ye, A.; He, Z.; Shang, Y. Quasi-static cyclic testing of elevated RC pile–cap foundation for bridge structures. *J. Bridge Eng.* **2016**, *21*, 04015042. [[CrossRef](#)]
19. Yilmaz, T.; Banerjee, S.; Johnson, P.A. Performance of Two Real-Life California Bridges under Regional Natural Hazards. *J. Bridge Eng.* **2016**, *21*, 1–15. [[CrossRef](#)]
20. Su, D.; Yan, W.M.; Bao, X.H.; Huang, S. Nondimensional solutions for laterally loaded piles in sand considering nonlinear soil–pile interactions. *Int. J. Geomech.* **2018**, *18*, 04018077. [[CrossRef](#)]
21. Mangalathu, S.; Heo, G.; Jeon, J.S. Artificial neural network based multi-dimensional fragility development of skewed concrete bridge classes. *Eng. Struct.* **2018**, *162*, 166–176. [[CrossRef](#)]
22. Alipour, A.; Shafei, B.; Shinozuka, M. Performance evaluation of deteriorating highway bridges located in high seismic areas. *J. Bridge Eng.* **2010**, *16*, 597–611. [[CrossRef](#)]
23. Scott, B.D.; Park, R.; Priestley, M.J.N. Stress–strain behavior of concrete confined by overlapping hoops at low and high strain rates. *ACI Struct. J.* **1982**, *79*, 13–27.
24. Caltrans. *Seismic Design Criteria, Version 2.0*; California Department of Transportation: Sacramento, CA, USA, 2014.
25. Silva, P.F.; Megally, S.; Seible, F. Seismic performance of sacrificial exterior shear keys in bridge abutments. *Earthq. Spectra* **2009**, *25*, 643–664. [[CrossRef](#)]
26. Duncan, J.M.; Mokwa, R.L. Passive earth pressures: Theories and tests. *J. Geotech. Geoenviron. Eng.* **2001**, *127*, 248–257. [[CrossRef](#)]
27. Douglas, D.J.; Davis, E.H. The movement of buried footings due to moment and horizontal load and the movement of anchor plates. *Geotechnique* **1964**, *14*, 115–132. [[CrossRef](#)]
28. Fang, Y.; Chen, T.; Wu, B. Passive earth pressures with various wall movements. *J. Geotech. Eng.* **1994**, *120*, 1307–1323. [[CrossRef](#)]
29. Matlock, H. Correlation for Design of Laterally Loaded Piles in Soft Clay. In *Proceedings of the Offshore Technology Conference*, Houston, TX, USA, 22–24 April 1970.
30. Frazier, P., Jr. Experimental and Analytical Studies of Behavior of Single Piles in Sand under Lateral and Axial Loading. Ph.D Thesis, The University of Texas at Austin, Austin, TX, USA, 1971.
31. API American Petroleum Institute. *Recommended Practice for Planning, Designing, and Constructing Fixed Offshore Platforms—Working Stress Design*; RP 2A–WSD; API American Petroleum Institute: Washington, DC, USA, 2005.
32. Reese, L.C.; O’Neill, M.W. *Drilled Shafts: Construction Procedures and Design Methods*; Report No. FHWA–HI–88–042; US Department of Transportation, Federal Highway Administration: Richmond, VA, USA, 1987.
33. Mosher, R.L. *Load Transfer Criteria for Numerical Analysis of Axially Loaded Piles in Sand*; US Army Engineering Waterways Experimental Station: Vicksburg, MS, USA, 1984.
34. Vijayvergiya, V.N. *Load–Movement Characteristics of Piles*; Proceedings, Ports 77; American Society of Civil Engineers: Reston, VA, USA, 1977; Volume 11, pp. 269–286.
35. Li, Z.X.; Yue, F.Q.; Zhou, L. Equivalent Kelvin impact model of bridge impact analysis in earthquake. *Eng. Mech.* **2008**, *25*, 128–133.
36. Malhotra, P.K. Response of buildings to near-field pulse-like ground motions. *Earthq. Eng. Struct. Dyn.* **1999**, *28*, 1309–1326. [[CrossRef](#)]
37. *GB18306–2015*; Seismic Ground Motion Parameter Zonation Map of China. China Standard Press: Beijing, China, 2015.

Disclaimer/Publisher’s Note: The statements, opinions and data contained in all publications are solely those of the individual author(s) and contributor(s) and not of MDPI and/or the editor(s). MDPI and/or the editor(s) disclaim responsibility for any injury to people or property resulting from any ideas, methods, instructions or products referred to in the content.